Fuel 375 (2024) 132616

Contents lists available at ScienceDirect

Fuel

journal homepage: www.elsevier.com/locate/fuel

Full length article

Ammonia as a fuel: Optical investigation of turbulent flame propagation of NH_3/Air and $NH_3/H_2/N_2$/Air flames at engine conditions

Marc Klawitter [a,*], Silas Wüthrich [b], Patrick Cartier [b], Patrick Albrecht [b], Kai Herrmann [b], Clemens Gößnitzer [c], Gerhard Pirker [c], Andreas Wimmer [a,c]

[a] Institute of Thermodynamics and Sustainable Propulsion Systems, Graz University of Technology, Graz, Austria
[b] Institute of Thermal and Fluid Engineering, University of Applied Sciences Northwestern Switzerland, Windisch, Switzerland
[c] LEC GmbH (Large Engines Competence Center), Graz, Austria

ARTICLE INFO

Keywords:
Ammonia
Partially cracked ammonia
Optical diagnostics
Optical engine test rig
Turbulent premixed combustion
Turbulent flame propagation
Effective Lewis number

ABSTRACT

Ammonia is a promising future energy carrier because of its carbon-free nature and high volumetric energy density compared to hydrogen. However, implementing ammonia as a fuel appears challenging due to its low reactivity. This can be improved, inter alia, by cofiring with a highly reactive fuel like hydrogen. A fuel mixture of ammonia, hydrogen, and nitrogen with favorable thermochemical properties can be produced by partially cracking ammonia. To assess the combustion behavior of ammonia and partially cracked ammonia at engine conditions, this study performs experiments on an optical engine test rig. Ammonia cracking ratios of 0, 7.5, and 10%, fuel-air equivalence ratios of 0.7 to 1.2, and different turbulence conditions at variable engine speeds are investigated at a compression pressure of 7 MPa. A turbulent flame speed approach is determined from high-speed schlieren imaging in the combustion chamber. The corresponding laminar flame properties and effective Lewis number are calculated numerically and the combustion regimes are assessed. The results show that ammonia/air flames propagate significantly faster under turbulent, engine-like conditions than expected from results at laminar, ambient conditions. Additionally, the partial cracking of ammonia further improves the turbulent combustion behavior. With lean fuel/air mixtures, a cracking ratio of 10% is sufficient to achieve flame speeds close to that of methane under highly turbulent flow conditions. The observed stronger influence of turbulence on the flame speed of ammonia and partially cracked ammonia compared to methane is due to the lower effective Lewis numbers and higher Karlovitz numbers of these fuels.

1. Introduction

Ammonia is a promising energy carrier due to its carbon-free nature and higher volumetric energy density than hydrogen. Before ammonia may be implemented as a fuel for combustion engines, its challenging thermochemical properties need to be studied thoroughly. In the development of combustion systems, not only long ignition delay times and low laminar burning velocities but also ammonia slip and potentially high emissions of nitrogen oxides and nitrous oxide must all be considered. The state of the art in large engine applications of gaseous fuels is represented by natural gas engines operating at lean conditions. Introducing new fuels to combustion systems challenges current storage methods, material and oil compatibility, injection strategies, and aftertreatment systems; it also impacts fundamental characteristics of the combustion process including mixture formation, ignition, and flame propagation. This has significant effects on the development of efficient, robust, and low-emission combustion processes, as well as on the simulation methods and models as an integral part of the development process.

To compensate for the challenging properties of ammonia as a fuel, a highly reactive fuel can be admixed. Hydrogen appears to be an attractive candidate since it is also carbon-free and can be directly produced from ammonia. For this, ammonia (NH_3) is separated into its components hydrogen (H_2) and nitrogen (N_2) by dissociation - so-called cracking. The cracking process can potentially be performed in situ [1,2]. The fuel mixture resulting from partial NH_3 cracking, $NH_3/H_2/N_2$, is called partially cracked NH_3 and will be investigated in this study along with pure NH_3 and CH_4.

With NH_3 and H_2, particular attention must be paid to the turbulent flame propagation. Hydrogen in particular exhibits a high molecular diffusivity. The effects of differential diffusion on turbulent flame propagation are extensively discussed in the literature, *e.g.* in [4,5]. Mixtures with an effective Lewis number below unity are subject to

* Correspondence to: Inffeldgasse 19, 8010 Graz, Austria.
E-mail address: klawitter@ivt.tugraz.at (M. Klawitter).

https://doi.org/10.1016/j.fuel.2024.132616
Received 1 June 2024; Received in revised form 17 July 2024; Accepted 24 July 2024
Available online 2 August 2024

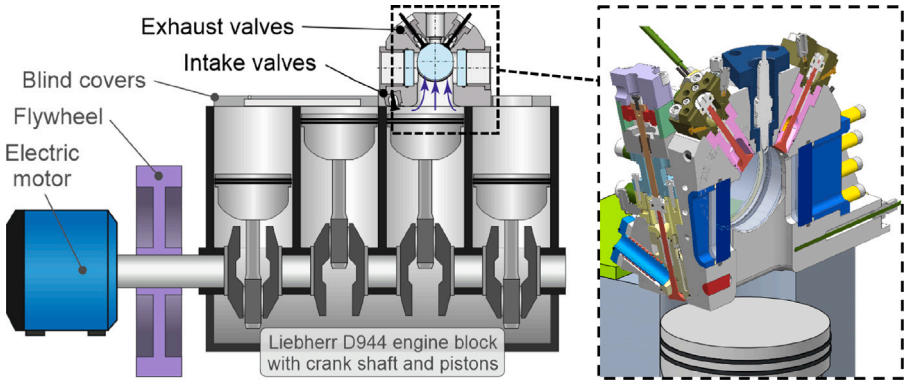

Fig. 1. Optical engine test rig "Flex-OeCoS", detailed view of the cylinder head including the optical access to the combustion chamber, inlet and outlet valves, and spark plug insert; for details, see [3].

increased flame propagation under turbulent conditions which is potentially caused by an enlargement of the flame surface area through thermodiffusive instabilities and an increase in local burning rates. This applies to both low turbulence and high turbulence flames [6]. Additionally, the low laminar burning velocity of ammonia corresponds to a large flame thickness, which enables turbulence to strongly influence flame propagation. The turbulence-related combustion behavior can therefore differ considerably from that of conventional fuels.

In recent years, several research groups have made progress in analyzing the fundamental phenomena governing the turbulent combustion of NH_3 and NH_3/H_2 blends [6–14]. Fan et al. [7] observed a linear increase of turbulent to laminar flame speed of NH_3/air flames with increasing turbulence intensity on a burner setup at high Karlovitz number conditions. Cai et al. [6] extended those results, emphasizing the significant role of differential diffusion in highly turbulent NH_3/H_2/air flames. Using fan-stirred constant volume combustion chambers, the results of Wang et al. [8], Dai et al. [14], and Xia et al. [9] support these findings and extend them to NH_3/air flames. Lhuillier et al. [10] found the enhancing effect of H_2 addition on turbulence response to decrease above a volumetric H_2 content of 10%. Zitouni et al. [11] link this behavior to a change in combustion regime from thin reaction zones to corrugated flamelets. These fundamental studies were all performed on burners or fan-stirred constant volume combustion chambers. While their relevance to engine applications is assured, these investigations are limited in initial temperatures and pressures or turbulence intensities.

In addition, the first studies investigating the flame propagation of NH_3 and NH_3 blends on optical engines have been published recently [15–17]. Zhang et al. [15] compared the flame propagation of NH_3 and CH_4, showing the lower combustion stability and thermal efficiency of NH_3. They found that while CH_4 combustion is mainly driven by temperature, NH_3 combustion is mainly driven by turbulence. Extending the investigations to hydrogen blends, Li et al. [16] found optima in H_2 blending content for thermal efficiency and combustion stability. Uddeen et al. [17] investigated ethanol and methane blending effects and found that ethanol blending caused higher flame propagation but also higher emissions. To the authors' knowledge, no studies have been published that present optical results to assess the effect of turbulence intensity on the flame speeds of ammonia and partially cracked ammonia at engine-like thermodynamic and flow conditions.

The effect of H_2 admixture on emission characteristics has been studied by Lhuillier et al. [18] on a spark-ignition engine with volumetric H_2 contents of 0–60%. They found a monotonic decrease in unburned NH_3 and a monotonic increase in NO_x emissions with increasing H_2 fuel fraction. Mercier et al. [19] extended these results by investigating H_2 admixture through NH_3 dissociation and confirmed the NH_3-NO_x trade-off with increasing NH_3 dissociation degree. Beyond that, they found N_2O and H_2 emissions to increase with the NH_3 dissociation degree increasing between 0–15%. These effects of H_2 admixture on the emission characteristics must be considered when assessing NH_3/H_2 fuel blends.

Given the aforementioned state of the art, this study focuses on the following objectives:

(1) Provide optical results of turbulent flame propagation of NH_3/air and partially cracked NH_3/air mixtures at engine-like compression temperatures, compression pressures, and flow and turbulence conditions.

(2) Determine the dominant combustion regimes of NH_3/air and partially cracked NH_3/air mixtures at the given engine conditions.

(3) Assess the flame propagation of NH_3/air and partially cracked NH_3/air mixtures in comparison to CH_4/air mixtures.

(4) Evaluate the turbulence effect on the different fuel/air mixtures and discuss the main causes.

(5) Determine the required NH_3 cracking ratio for flame speeds comparable to corresponding CH_4/air mixtures.

2. Methodology

2.1. Experimental setup

The flame propagation of the investigated gas mixtures is captured on the "Flex OeCoS" optical test rig, see Fig. 1. Based on a four-cylinder engine block with a driven crankshaft, one cylinder of 1990 cm^3 displacement is equipped with a cylinder head specifically designed to provide optical access to the initial flame propagation zone and a fully variable valve train. The optical access to the combustion chamber is provided by two windows of 60 mm diameter in the main optical axis. A detailed description of the test rig is found in [3]. The test rig is designed to reach engine-like thermodynamic, flow, and turbulence conditions while ensuring excellent optical access.

Simultaneous high-speed schlieren and chemiluminescence imaging is applied in the main optical axis. The temporal resolution is set to 0.1 °CA at engine speeds n of 400 and 600 min^{-1} and 0.2 °CA at engine speeds of 800 and 1000 min^{-1}. The spatial resolution of the schlieren imaging is 9.24 pixel/mm in this setup. The chemiluminescence of various species can be visualized by using interchangeable optical filters. In this study, a 308 nm narrowband filter for OH^* radical radiation is applied. The optical setup shown in Fig. 2 is identical to the setup in [20,21].

The flow and turbulence conditions in the combustion chamber at engine speeds of 400, 600, and 800 min^{-1} have been studied previously using planar high-speed particle image velocimetry (PIV) measurements in air [3]. The following considers the results of the crank-angle resolved, ensemble-averaged (N = 200 cycles), and spatially averaged mean flow velocity u and turbulence intensity u'. The turbulence intensity is defined as the root mean square value of the turbulent fluctuation velocity. Fig. 3 shows u and u' at different engine speeds in the relevant crank angle range. At all engine speeds, considerable flow velocities

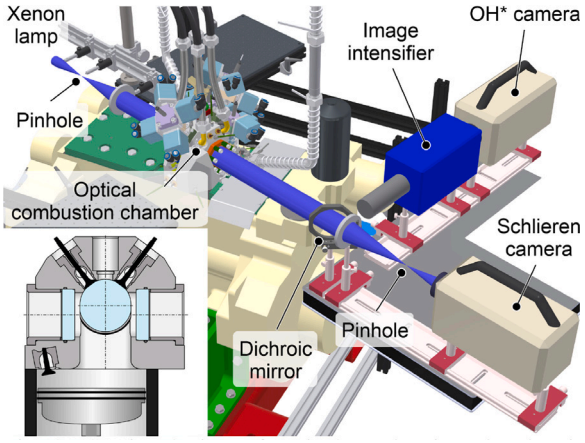

Fig. 2. Sectional view of optical combustion chamber in main optical direction and overview of optical setup for simultaneous schlieren and chemiluminescence imaging including light source, collimating lens, experimental area, dichroic mirror, converging lens, pinhole, bandpass filter, image intensifier, two high-speed cameras; light beam in blue. (For interpretation of the references to color in this figure legend, the reader is referred to the web version of this article.)
Source: Figure adapted from [21].

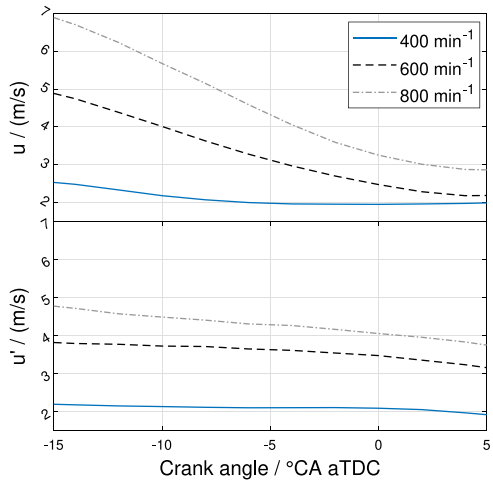

Fig. 3. Ensemble-averaged (N = 200 cycles) and spatially averaged mean flow velocity u and turbulence intensity u' as functions of crank angle; n = [400, 600, 800] min^{-1}, p_c = 10 MPa; T_{in} = 473 K; for details, see [3].

are present within the evaluation range. The pressure level has been shown to have no significant influence on u and u'; the determining factor is engine speed [3]. Therefore, the PIV results obtained at a compression pressure p_c of 10 MPa are applied to the 7 MPa cases in this study. To obtain single characteristic values at each engine speed, the data are also averaged temporally. The crank angle range of the corresponding flame speed evaluation is applied. Measurements at an engine speed of 1000 min^{-1} are not characterized for mean flow velocity and turbulence intensity.

In addition, the longitudinal integral length scales L_I are determined from the integral of the spatial autocorrelation function of the fluctuation velocity in accordance with [22]. The mean values for L_I on the investigated 2D plane are estimated to be 12.0, 13.8, and 14.8 mm at engine speeds of 400, 600, and 800 min^{-1}, respectively.

The thermodynamic conditions are characterized by in-cylinder pressure measurements in the present study and gas temperature measurements under cold flow conditions in earlier studies [3,20]. The gas temperature is reconstructed from fine wire thermocouple measurements with sensor wire diameters $\leq$ 25 µm. The determined temperature profiles are used for the numerical calculation of fuel properties at the given engine conditions, see Section 2.3.

The investigated fuels are ammonia (NH_3), partially cracked ammonia (crNH_3), and methane (CH_4). In this study, the degree of dissociation of NH_3 is referred to as the cracking ratio γ. It defines the molar fraction χ of NH_3 that is dissociated into H_2 and N_2 and is calculated by Eq. (1). Table 1 indicates the investigated NH_3 cracking ratios and corresponding molar fractions in the fuel mixture. Low cracking ratios are targeted since an excessive increase of γ can reduce the global system efficiency and increase emissions of NO_x, N_2O, and H_2 [18,19]. CH_4 serves as a reference as it is the main component in natural gas. The fuel gas mixture is supplied by two injectors per intake port with one feeding NH_3 and one feeding a 3:1 mixture of H_2 and N_2 into the intake port. The fuel mixture of a specific NH_3 cracking ratio is achieved by adjusting the energizing times of the two injectors.

$$\gamma = \frac{\chi_{H_2}}{3/2 * \chi_{NH_3} + \chi_{H_2}} \quad (1)$$

Table 2 lists the investigated fuel-air mixtures and boundary conditions. Equal operating conditions for all fuels are targeted for comparability. However, restrictions on the operability of the engine test rig cause restrictions or deviations in the operation conditions with

Table 1
Investigated NH_3 cracking ratios γ and corresponding molar fractions χ in fuel.

γ/(%)	χ_{NH_3}/(%)	χ_{H_2}/(%)	χ_{N_2}/(%)
0.0	100.0	0.0	0.0
7.5	86.1	10.5	3.5
10.0	81.8	13.6	4.6

the different fuels. The fuel-air equivalence ratios ϕ are limited to a minimum of 0.7 due to the flammability limit of NH_3. The compression pressure p_c, which refers to the peak combustion chamber pressure with motored engine operation, is set to 7 MPa for all cases as this offers engine-relevant conditions regarding in-cylinder temperature and pressure and limits knocking in the CH_4 cases. For this, the inlet air pressure is set between 0.19 and 0.34 MPa dependent on the engine speed. The inlet air temperature T_{in} in CH_4 cases is set to 323 K to limit knocking. To account for the high autoignition temperature of NH_3, the inlet air temperature with NH_3 and crNH_3 is set to 373 K. The corresponding gas temperatures at ignition timing are given in Table 3. The engine speeds of 400–1000 min^{-1} are chosen to reach flow conditions similar to typical engine operation conditions. As presented in Fig. 3, the mean flow velocity and the turbulence intensity reach magnitudes comparable to literature references of spark-ignition engines [23,24]. The fuel injection timing is set to −470 °CA after the fired top dead center (aTDC) at 400 and 600 min^{-1} and is advanced to −570 °CA aTDC at 800 and 1000 min^{-1} to ensure homogenization of the fuel/air mixture. The ignition timing IT is fixed for all gas mixtures to −15 °CA aTDC for stable combustion of NH_3/air mixtures. With CH_4 operating points, this early ignition timing causes knocking at low engine speeds of 400 min^{-1}, which prevents measurements in these cases. All of the fuel/air mixtures are reliably ignited by spark ignition.

2.2. Image evaluation method

The flame speed is determined from the optical schlieren data. The image evaluation method is based on the time and crank angle-resolved detection of the flame contour on the schlieren images. Due to the density gradients in the unburned gas caused by the high turbulence levels, detection of the flame contour based on threshold values leads to errors. Thus, the detection is based on predefined probability density functions for the burned and unburned zones with which pixel values are assigned to one of the zones. The projected flame area is determined from the detected flame contour. The assumption of a spherical flame is not valid under the given engine conditions, so the flame speed

Table 2
Fuel-air mixtures and boundary conditions investigated on the engine test rig.

Parameter/(unit)	Value
NH_3 cracking ratio γ/(%)	0.0; 7.5; 10.0
Fuel-air equivalence ratio ϕ/(–)	0.70–1.20
Compression pressure p_c/(MPa)	7.0
Inlet air temperature T_{in}/(K)	NH_3, $crNH_3$: 373 CH_4: 323
Engine speed n/(min^{-1})	400; 600; 800; 1000
Fuel injection timing/(°CA aTDC)	400–600 min^{-1}: −470 800–1000 min^{-1}: −570
Ignition timing IT/(°CA aTDC)	−15
Compression ratio ε/(–)	13.27
Displacement volume/(cm^3)	1990

may not be determined as the time derivative of an area-equivalent radius. Instead, the projected flame area difference per time step is determined and divided by the actual flame front circumference to obtain an average propagation distance. The time derivative of this distance is referred to as flame speed.

To determine the characteristic turbulent flame speeds of the different fuel mixtures and boundary conditions, firstly a temporal average is calculated for each cycle of a measurement point. For this, the evaluation range is limited to a minimum area-equivalent flame radius of 5 mm. This excludes the initial flame propagation that is significantly influenced by the ignition energy. The maximum flame radius is limited to 20 mm to limit the influences of pressure rise and chamber interaction on flame propagation. Using the temporally averaged flame speeds of each cycle, 20 cycles per measurement point are ensemble-averaged to obtain the characteristic turbulent flame speed of this measurement point. The standard deviations are given as error bars in the results.

The resulting flame speed is hereafter referred to as apparent turbulent flame speed s_T^a. Due to the given thermodynamic and flow conditions, the captured flame propagation is specific to the test rig. In particular, the significant background flow influences the magnitude of the acquired flame speed. By this, the effect of flame stretch cannot be compensated for by extrapolation to zero stretch either. Thus, the results do not represent the gas mixture-specific turbulent burning velocity s_T, and literature results from different test rigs may vary. The potentially higher flame speed determined from line-of-sight integrated schlieren images compared to 2D-cut laser tomography has to be considered further [25]. Therefore, a qualitative comparison of the response of the various fuel mixtures to the thermodynamic and flow conditions will be made and fundamental combustion behavior can be observed.

The apparent turbulent flame speed s_T^a refers to the burned gas. Analogous to the determination of the laminar burning velocity, s_T^a is transposed to the unburned side by the burned to unburned gas density ratio ρ_b/ρ_u, see Eq. (2). This gives the unburned apparent turbulent flame speed $s_{T,u}^a$.

$$s_{T,u}^a = \frac{\rho_b}{\rho_u} s_T^a \tag{2}$$

This study uses OH^* chemiluminescence optical data solely to visualize OH^* radicals formed during the combustion process; the following results do not include them. In further studies, the OH^* data will be used to derive ignition delay times.

2.3. Numerical evaluation of fundamental fuel/air mixture properties

All the following properties of the gas mixtures are determined by applying the chemical kinetics solver Cantera [26]. For fuel/air mixtures containing NH_3 and H_2, the latest NH_3 reaction mechanism of Stagni et al. is applied [27]. According to a recent study by Szanthoffer et al. applying a large collection of experimental data on laminar burning velocity, ignition delay time, and species concentrations [28], this mechanism is one of the best-performing mechanisms for NH_3 and NH_3/H_2 combustion. Additionally, the mechanism is compared to four other well-performing mechanisms [29–32] at the conditions of the present study in the supplementary material S4 and is considered suitable for the present study. For CH_4/air mixtures, the well-established CRECK high-temperature C1–C3 mechanism is applied [33].

A one-dimensional freely propagating flame model of Cantera is applied to obtain the laminar burning velocity $s_{L,u}^0$ of the gas mixtures. The laminar flame thickness l_F is determined by Eq. (3). The thermal conductivity λ and the specific heat capacity c_p are evaluated at the temperature of the maximum gradient in the temperature profile of the one-dimensional flame. The density ρ and $s_{L,u}^0$ are evaluated at the unburned gas conditions [34]. To determine the density ratio ρ_b/ρ_u required for calculating $s_{T,u}^a$, the burned gas density is evaluated at the adiabatic isobaric equilibrium in Cantera.

$$l_F = \frac{(\lambda/c_p)_0}{(\rho s_L^0)_u} \tag{3}$$

Several approaches have been suggested for deriving the effective Lewis number Le_{eff} of a premixed flame from the Lewis number values of each present species, *e.g.*, [35,36]. Bechtold and Matalon [35] introduce a formulation of Le_{eff} based on the Lewis numbers of the deficient reactant Le_D and the excessive reactant Le_E, see Eq. (4). This formulation is applied in the present study since it is also valid with fuel/air mixtures close to stoichiometry. Here, A is a weighting coefficient based on the parameter Φ_{BM} and the Zeldovich number β of the mixture. Φ_{BM} is equal to the equivalence ratio Φ for rich and stoichiometric mixtures and equal to the reciprocal of the equivalence ratio for lean mixtures. Thereby, Φ_{BM} is defined as equal or larger than unity. β is evaluated following the approach of Beeckmann et al. [37]. For fuel mixtures, the fuel Lewis number is determined by volumetric fraction weighting of the Lewis numbers of the individual fuels [38].

$$\begin{aligned} &Le_{eff} = 1 + \frac{(Le_E - 1) + (Le_D - 1)A}{1 + A}, \\ &\text{with } A = 1 + \beta(\Phi_{BM} - 1), \\ &\begin{cases} \Phi \geq 1: & \Phi_{BM} = \Phi \\ \Phi < 1: & \Phi_{BM} = 1/\Phi \end{cases} \end{aligned} \tag{4}$$

The in-cylinder conditions at the time of ignition are taken as the initial conditions for the calculation. The initial pressure and gas composition are set according to the present experimental results. The initial temperature has been determined using an in-house 0D simulation tool. The results of the simulations are validated against temperatures derived from previous fine wire thermocouple measurements of air and NH_3/air mixtures in the combustion chamber of the test rig [3,20].

3. Discussion of results

This section presents and discusses the results of the experiments and numerical calculations performed. The data set is available in the supplementary material S1–S3. For the following fuel comparisons, the inlet air temperature difference between 323 K with CH_4 and 373 K with NH_3 and $crNH_3$ affects the flame speeds mainly by the influence on the laminar burning velocity. While deviating initial conditions limit direct comparability, the results are more significant in the application of these fuels in combustion engines as they respect the operation limitations due to ignitability and knocking. For reasons of readability, this difference will not be stated for each comparison.

3.1. Laminar burning velocity and effective Lewis number results

Fig. 4 presents the reaction kinetic results of $s_{L,u}^0$ and Le_{eff} as a function of the equivalence ratio of NH_3/air, $crNH_3$/air (γ = 7.5% and 10%), and CH_4/air mixtures. The initial conditions for the calculations

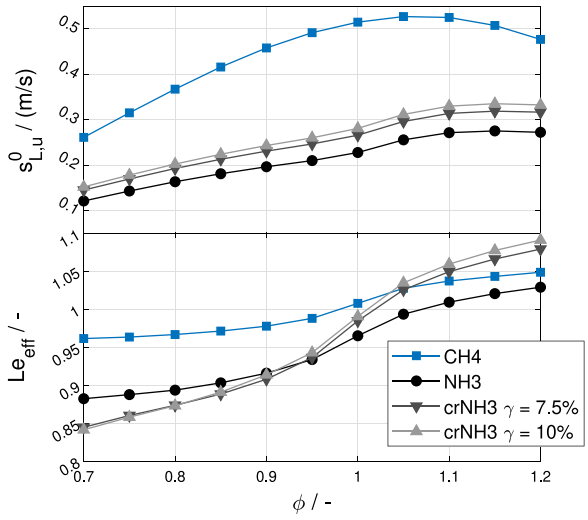

Fig. 4. Laminar burning velocity $s^0_{L,u}$ and effective Lewis number Le_{eff} as a function of the equivalence ratio ϕ with NH_3, $crNH_3$ (γ = 7.5% and 10%), and CH_4; initial conditions according to ignition conditions, see Table 3.

Table 3
Initial temperature T_{IT} and pressure p_{IT} at ignition timing conditions for numerical calculation of fuel/air mixture properties.

Fuel	T_{IT} (K)	p_{IT} (MPa)
CH_4	750	5.0
NH_3	794	4.8
$crNH_3$, γ = 7.5%	786	4.8
$crNH_3$, γ = 10%	784	4.8

are set to the thermodynamic state at ignition timing of −15 °CA aTDC. Due to the different inlet conditions and mixture properties of the fuels, the initial conditions also differ as presented in Table 3.

The laminar burning velocity of all fuels peaks with slightly rich mixtures and strongly decreases with increasingly lean mixtures. Under laminar conditions, CH_4 propagates around 75% to 135% faster than NH_3 at ignition conditions. Despite this substantial difference, ammonia performs significantly better at engine-like temperatures and pressures than expected from the frequently cited ambient results, which yield a $s^0_{L,u}$ of CH_4 five times higher than of NH_3. This is in agreement with literature that shows a smaller pressure exponent and larger temperature exponent of NH_3 compared to CH_4 in correlations for $s^0_{L,u}$ [39]. A partial NH_3 cracking of 10% increases the $s^0_{L,u}$ by at least 20% and up to 25% with very lean mixtures.

The Le_{eff} of CH_4 is close to unity with all equivalence ratios; the effect of the equivalence ratio on the Le_{eff} of CH_4 is weak. While the effect on NH_3 is more pronounced, the Le_{eff} of NH_3 is generally lower than that of CH_4, indicating a stronger differential diffusion. With very lean mixtures, the effective Lewis number approaches the Lewis number of the fuel. Partially cracked ammonia contains hydrogen with a high mass diffusivity. This causes a rapid decrease of the effective Lewis number with increasingly lean mixtures of $crNH_3$.

3.2. Turbulent combustion regimes

To characterize the interaction of the turbulent flow with the flame front, the turbulent combustion regimes present in the combustion chamber are estimated using the turbulence scales u' and L_I, which are determined from previous PIV investigations, and the flame scales $s^0_{L,u}$ and l_F, which are determined numerically. Representative measurement points are displayed on a Borghi–Peters diagram in Fig. 5 by the velocity ratio $u'/s^0_{L,u}$ and the length scale ratio L_I/l_F. The turbulent

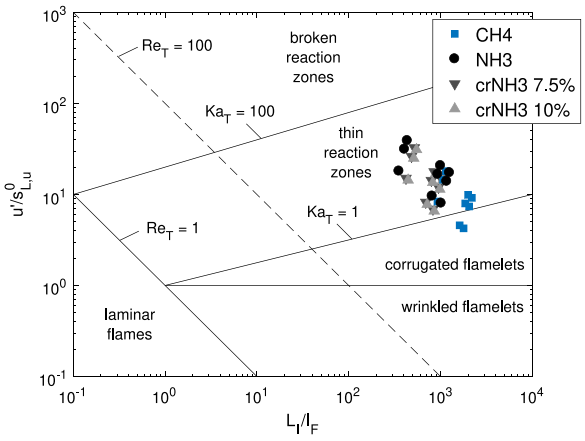

Fig. 5. Borghi–Peters diagram of premixed turbulent combustion regimes with ignition conditions of representative measurement points in this study (NH_3/air, $crNH_3$/air (γ = 7.5% and 10%) and CH_4/air mixtures; n = [400, 600, 800 min^{-1}]; ϕ = [0.7, 1.0, 1.2]; p_c = 7 MPa; T_{in,CH_4} = 323 K; T_{in,NH_3} = $T_{in,crNH_3}$ = 373 K).

Reynolds number $Re_T = (u'/s^0_{L,u})\cdot(L_I/l_F)$ and Karlovitz number $Ka_T = (u'/s^0_{L,u})^{3/2}\cdot(L_F/l_I)^{1/2}$ are indicated by isolines.

All measurement points are located in the central right area of the regime diagram due to the high L_I of 12.0–14.8 mm on this test rig and the low l_F of all fuels at ignition conditions. The CH_4 measurement points are located between the regimes of corrugated flamelets and thin reaction zones with a Karlovitz number around unity. Here, turbulence interacts with the thin flame by corrugating the flame surface. However, even the smallest turbulent scales are of a similar size to the flame thickness and barely enter and perturb the flame structure [34].

The NH_3 measurement points are shifted to higher Karlovitz numbers by a higher l_F and lower $s^0_{L,u}$ compared to CH_4. They are all located in the thin reaction zone, indicating that the smallest eddies enter and widen the preheat zone of the flame. The reaction zone remains too thin to be perturbed in this regime [34]. Increasing the NH_3 cracking ratio and thereby the H_2 content yields results closer to the corrugated flamelets regime, which is in agreement with the findings of Zitouni et al. [11].

An increased flame-turbulence interaction of NH_3 is evident from the qualitative difference of combustion regimes of the CH_4 and NH_3 flames. The effect on turbulent flame propagation is discussed in the following sections.

3.3. Schlieren imaging results

Fig. 7 shows schlieren imaging sequences of exemplary combustion cycles with (a) CH_4/air, (b) NH_3/air, (c) $crNH_3$/air (γ = 7.5%), and (d) $crNH_3$/air (γ = 10%) at ϕ = 1.00 and n = 600 min^{-1}. The corresponding videos are provided in the supplementary material S5. The ignition at an IT of −15 °CA aTDC is followed by an ignition delay phase without observable flame propagation and a subsequent rapid flame propagation. The long ignition delay of NH_3 is apparent at −13 °CA aTDC. While an initial flame kernel has developed with CH_4, NH_3 has not ignited visibly. Partial NH_3 cracking shortens the ignition delay as visible in (c) and (d). Similarly, the significantly slower flame propagation of NH_3 compared to CH_4 at n = 600 min^{-1} is observable comparing (a) and (b). Although partial NH_3 cracking accelerates the flame propagation, $crNH_3$ (γ = 10%) propagates significantly slower than CH_4 at the given equivalence ratio and engine speed.

In combustion cycle (a), the flame shape is close to spherical. Due to the cyclic fluctuations of the flow conditions in the combustion chamber, the shape can strongly diverge from spherical as apparent

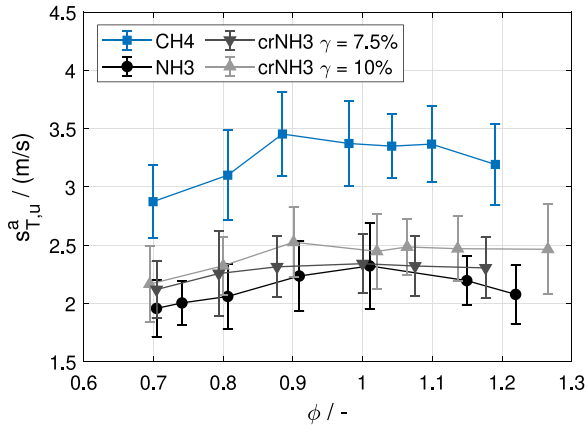

Fig. 6. Unburned apparent turbulent flame speed $s^{a}_{T,u}$ as a function of the equivalence ratio ϕ with NH_3/air, $crNH_3$/air (γ = 7.5% and 10%), and CH_4/air mixtures; n = 600 min^{-1}; p_c = 7 MPa; T_{in,CH_4} = 323 K; T_{in,NH_3} = $T_{in,crNH_3}$ = 373 K.

in cycles (b), (c), and (d). Therefore, a spherical flame front may not be assumed. Strong interaction with the background flow influences the apparent flame propagation speed results. The flame-turbulence interaction is evident in the small-scale wrinkled flame front.

3.4. Turbulent flame propagation results

Fig. 6 shows the unburned apparent turbulent flame speed as a function of the equivalence ratio with NH_3/air, $crNH_3$/air (γ = 7.5% and 10%), and CH_4/air mixtures. The displayed engine speed of 600 min^{-1} corresponds to an approximate turbulence intensity of 3.7 m/s.

The maximum flame speed of the fuels shifts from slightly rich mixtures under laminar conditions to stoichiometric or slightly lean mixtures under turbulent conditions. With increasingly lean mixtures, the decrease in $s^{a}_{T,u}$ is significantly less pronounced than in $s^{0}_{L,u}$ with all fuels. While $s^{0}_{L,u}$ decreases from ϕ = 1.0 to ϕ = 0.7 by 45–49% with all fuels, the decrease in $s^{a}_{T,u}$ remains within 9–16%. Specifically, the $s^{a}_{T,u}$ of $crNH_3$ (γ = 7.5% and 10%) decreases by only 9–11%, which shows improved relative flame speeds of $crNH_3$ compared to NH_3 and CH_4 with lean mixtures under turbulent conditions. The flame propagation of CH_4 remains around 50% faster than that of NH_3 at an engine speed of 600 min^{-1}. Partial NH_3 cracking of 10% increases $s^{a}_{T,u}$ by approximately 10% to 20% compared to NH_3. All these observations indicate an increasing turbulence effect on the flame speed of fuel/air mixtures with a decreasing effective Lewis number.

In stoichiometric mixtures, a cracking ratio of 7.5% shows no significant increase in $s^{a}_{T,u}$ compared to NH_3. Partial cracking increases the reactivity through the contained H_2 as evident from the $s^{0}_{L,u}$. However, partial cracking also increases the Le_{eff} of stoichiometric and rich mixtures, see Fig. 4. Additionally, the Ka_T of NH_3 is slightly higher than that of $crNH_3$. As a result, the stronger turbulence effect on NH_3 compensates for the enhanced reactivity of $crNH_3$ (γ = 7.5%). As mixtures become increasingly lean or rich, the increase in $s^{a}_{T,u}$ from partial cracking of NH_3 becomes more distinct. In rich mixtures, the $s^{a}_{T,u}$ of $crNH_3$ is nearly constant, which is caused by a decreasing flame speed of the contained NH_3 with increasingly rich mixtures but an increasing flame speed of the contained H_2, whose $s^{0}_{L,u}$ peaks at an equivalence ratio of 1.6 to 1.8 [32].

Fig. 8 shows the unburned apparent turbulent flame speed as a function of turbulence intensity at equivalence ratios of 0.8 and 1.0 with NH_3/air, $crNH_3$/air (γ = 7.5% and 10%), and CH_4/air mixtures. The turbulence intensity is varied by an engine speed variation of 400, 600, and 800 min^{-1}. With CH_4, knocking at 400 min^{-1} limits the engine speeds that can be investigated. Depending on the flame speed, the evaluated crank angle range and thus the flow and turbulence conditions vary slightly as indicated by the differing turbulence intensities in Fig. 8.

$s^{a}_{T,u}$ increases monotonically as turbulence intensity increases with all fuel/air mixtures. Under stoichiometric conditions, the difference in $s^{a}_{T,u}$ between CH_4 and NH_3 decreases from approximately 50% to 35% between u' = 3.7 and u' = 4.4. This supports a stronger turbulence effect on NH_3/air flames at the respective operation conditions, as expected from the lower Le_{eff} and higher Ka_T. This is also consistent with the findings of Zhang et al. [15] that NH_3 combustion is mainly driven by turbulence while CH_4 is mainly driven by temperature through its $s^{0}_{L,u}$. Furthermore, partial NH_3 cracking of 10% yields an increase in $s^{a}_{T,u}$ of around 10%.

With the lean mixtures at ϕ = 0.8, these trends are more pronounced. The difference between CH_4 and NH_3 decreases from 50% to 30% between u' = 3.7 m/s and u' = 4.4 m/s. The $crNH_3$ (γ = 10%) case shows a rather constant increase of around 15% compared to NH_3; a difference in $s^{a}_{T,u}$ of only 10% remains between CH_4 and $crNH_3$ (γ = 10%) at u' = 4.4 m/s. This shows that in highly turbulent engine applications, a cracking ratio as low as 10% can be sufficient to achieve flame speeds close to CH_4. Several investigations of engine applications confirm this range of required hydrogen addition [16,40,41]. This is in strong contrast to the results of experimental investigations on laminar burning velocities of $crNH_3$ at ambient conditions, suggesting cracking ratios of 40% for similar $s^{0}_{L,u}$ of CH_4 and $crNH_3$ [42,43].

With $crNH_3$ (γ = 10%), there is no significant difference in $s^{a}_{T,u}$ between ϕ = 0.8 and ϕ = 1.0. This implies that the enhanced turbulence effect can compensate for the equivalence ratio effect on the flame propagation of the lean mixture.

It should be noted that on the present test rig, the magnitude of $s^{a}_{T,u}$ is influenced not only by the turbulence intensity as engine speed increases but also by the mean flow velocity, as discussed in Section 2.2. The interaction of the flame front with the background flow is apparent in Fig. 7. Therefore, correlations for s_T from the literature (*e.g.*, [6,8,10,14]) do not apply to $s^{a}_{T,u}$. However, the influence of the mean flow velocity on flame speed remains unchanged with different fuels and equivalence ratios. The aforementioned relative behavior of the fuel/air mixtures is thus caused by the differing turbulence-flame interaction.

Existing studies have shown that the turbulence response of NH_3 and $crNH_3$/air flames is stronger than that of CH_4/air flames in fundamental investigations, *e.g.*, on constant volume combustion chambers [8,10]. The results in Fig. 8 show that this differing turbulence response is also significant at engine-like conditions and that the turbulence response contributes significantly to the absolute flame propagation speed of NH_3 and $crNH_3$ at engine-like conditions.

4. Conclusions

The turbulent flame propagation of NH_3/air, partially cracked NH_3/air, and CH_4/air mixtures under engine conditions is captured on an engine test rig with an optically accessible combustion chamber by applying schlieren imaging. The experimental results are compared to numerical results of the laminar burning velocity and effective Lewis number and the combustion regimes are assessed. The main conclusions are as follows:

(1) NH_3/air flames propagate faster under turbulent, engine-like conditions than expected from results at laminar, ambient conditions. This is due to a favorable response to high temperature, pressure, and turbulence levels. Partial cracking of NH_3 further improves the turbulent combustion behavior.

(2) With lean fuel/air mixtures, an NH_3 cracking ratio of 10% is sufficient to achieve flame speeds close to CH_4 under highly turbulent flow conditions.

(3) The observed stronger influence of turbulence on the flame speed of NH_3 and cracked NH_3 compared to CH_4 is caused firstly by

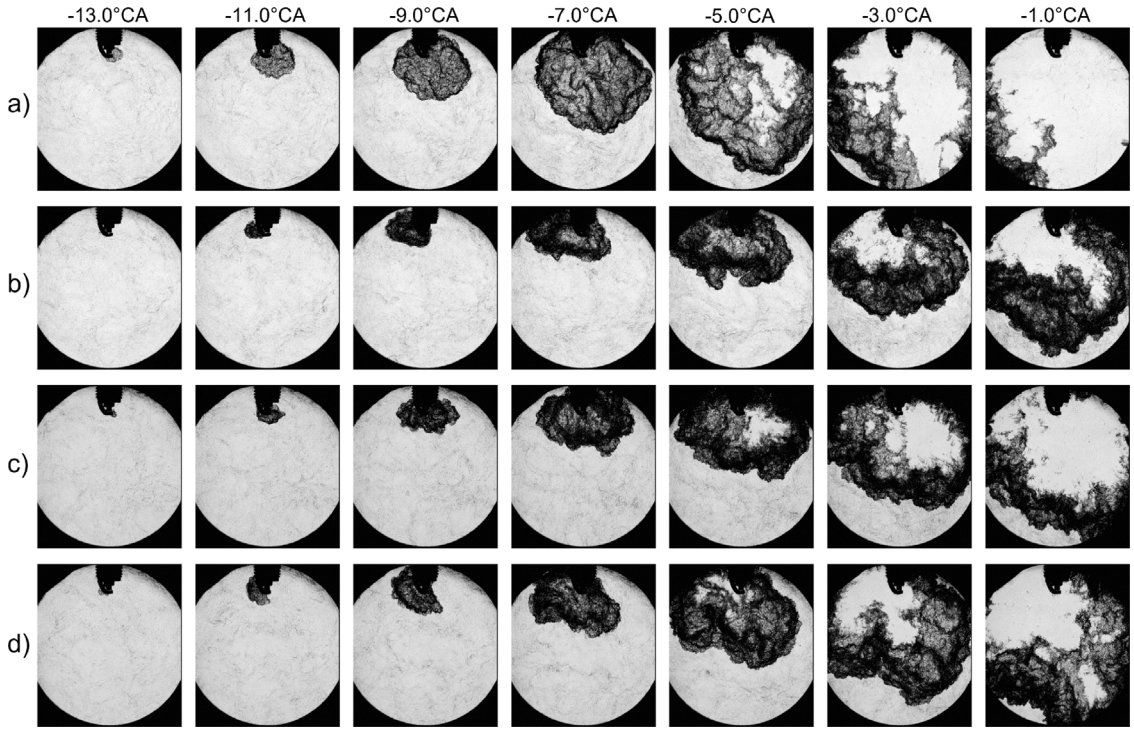

Fig. 7. Schlieren image sequences of exemplary combustion cycles: (a) CH_4/air, (b) NH_3/air, (c) $crNH_3$/air (γ = 7.5%), (d) $crNH_3$/air (γ = 10%); ϕ = 1.00; n = 600 min^{-1}; p_c = 7 MPa; T_{in,CH_4} = 323 K; T_{in,NH_3} = $T_{in,crNH_3}$ = 373 K; videos are provided in the supplementary material S5.

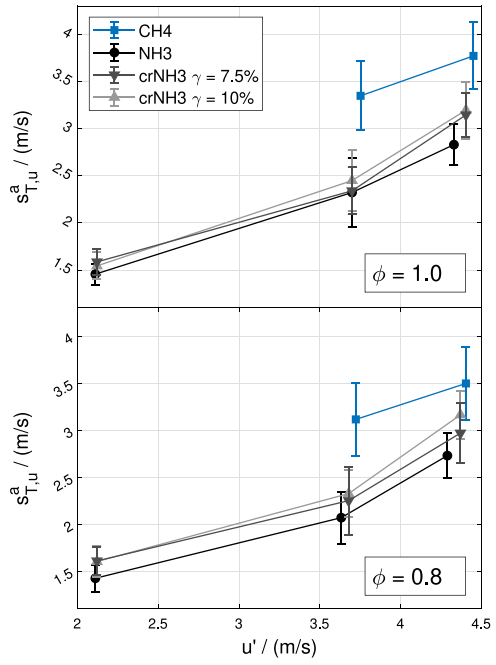

Fig. 8. Unburned apparent turbulent flame speed $s^a_{T,u}$ as a function of turbulence intensity u' with NH_3/air, $crNH_3$/air (γ = 7.5% and 10%), and CH_4/air mixtures; ϕ = 0.8 and 1.0; p_c = 7 MPa; T_{in,CH_4} = 323 K; T_{in,NH_3} = $T_{in,crNH_3}$ = 373 K.

the lower effective Lewis numbers of these fuels and secondly by the higher Karlovitz numbers, which place them in the thin reaction zones regime.

The findings regarding the turbulence effect obtained from research conducted on the present engine test rig are in agreement with the findings from fundamental investigations on burners and constant volume combustion chambers and extend their validity to engine-like thermodynamic and flow conditions. Future complementary CFD simulation will help to gain a deeper understanding of the turbulence-flame interaction and the influence of background flow on flame propagation at engine conditions.

For implementing ammonia as a fuel, the findings imply that ammonia and especially partially cracked ammonia are promising candidates for fueling internal combustion engines due to their favorable response to high temperature, pressure, and turbulence levels. Improvements in efficiency and stability of ammonia combustion are achievable not only through higher compression ratios, for example, but also by an engine design with increased turbulence generation. The remaining challenges in implementing ammonia as a fuel beyond the scope of this study include carbon-free synthesis, cost-competitiveness, safety regulations, material compatibility, engine system optimization, and emissions mitigation.

CRediT authorship contribution statement

Marc Klawitter: Writing – original draft, Visualization, Validation, Methodology, Investigation. **Silas Wüthrich:** Writing – review & editing, Visualization, Methodology, Investigation. **Patrick Cartier:** Validation, Software, Formal analysis, Data curation. **Patrick Albrecht:** Writing – review & editing, Investigation. **Kai Herrmann:** Writing – review & editing, Supervision, Resources, Funding acquisition, Conceptualization. **Clemens Gößnitzer:** Writing – review & editing, Supervision. **Gerhard Pirker:** Writing – review & editing, Supervision, Project administration. **Andreas Wimmer:** Supervision, Resources, Funding acquisition, Conceptualization.

Declaration of competing interest

The authors declare that they have no known competing financial interests or personal relationships that could have appeared to influence the work reported in this paper.

Data availability

Data will be made available on request.

Acknowledgments

The authors would like to acknowledge the financial support of the "COMET - Competence Centers for Excellent Technologies" Program of the Austrian Federal Ministry for Climate Action, Environment, Energy, Mobility, Innovation and Technology (BMK) and the Austrian Federal Ministry of Labor and Economy (BMAW) and the Provinces of Salzburg, Styria and Tyrol for the COMET Centre (K1) LEC GETS. The COMET Program is managed by the Austrian Research Promotion Agency (FFG).

Furthermore, financial support from the Swiss Federal Office of Energy (SFOE) and funding by Winterthur Gas & Diesel (WinGD) is gratefully acknowledged.

Appendix A. Supplementary data

Supplementary material related to this article can be found online at https://doi.org/10.1016/j.fuel.2024.132616.

References

[1] Comotti M, Frigo S. Hydrogen generation system for ammonia–hydrogen fuelled internal combustion engines. Int J Hydrog Energy 2015;40(33):10673–86. http://dx.doi.org/10.1016/j.ijhydene.2015.06.080.

[2] Liu J, Liu Z. In-cylinder thermochemical fuel reforming for high efficiency in ammonia spark-ignited engines through hydrogen generation from fuel-rich operations. Int J Hydrog Energy 2024;54:837–48. http://dx.doi.org/10.1016/j.ijhydene.2023.08.146.

[3] Schneider B, Schürch C, Boulouchos K, Herzig S, Hangartner M, Humair D, et al. The Flex-OeCoS—a novel optically accessible test rig for the investigation of advanced combustion processes under engine-like conditions. Energies 2020;13(7):1794. http://dx.doi.org/10.3390/en13071794.

[4] Lipatnikov AN, Chomiak J. Molecular transport effects on turbulent flame propagation and structure. Prog Energy Combust Sci 2005;31(1):1–73. http://dx.doi.org/10.1016/j.pecs.2004.07.001.

[5] Berger L, Attili A, Pitsch H. Synergistic interactions of thermodiffusive instabilities and turbulence in lean hydrogen flames. Combust Flame 2022;244:112254. http://dx.doi.org/10.1016/j.combustflame.2022.112254.

[6] Cai X, Fan Q, Bai X-S, Wang J, Zhang M, Huang Z, et al. Turbulent burning velocity and its related statistics of ammonia–hydrogen–air jet flames at high Karlovitz number: Effect of differential diffusion. Proc Combust Inst 2023;39(4):4215–26. http://dx.doi.org/10.1016/j.proci.2022.07.016.

[7] Fan Q, Liu X, Cai X, Brackmann C, Alden M, Bai X-S, et al. Structure and scalar correlation of ammonia/air turbulent premixed flames in the distributed reaction zone regime. Combust Flame 2022;241:112090. http://dx.doi.org/10.1016/j.combustflame.2022.112090.

[8] Wang S, Elbaz AM, Wang G, Wang Z, Roberts WL. Turbulent flame speed of NH3/CH4/H2/H2O/air-mixtures: effects of elevated pressure and Lewis number. Combust Flame 2023;247:112488. http://dx.doi.org/10.1016/j.combustflame.2022.112488.

[9] Xia Y, Hashimoto G, Hadi K, Hashimoto N, Hayakawa A, Kobayashi H, et al. Turbulent burning velocity of ammonia/oxygen/nitrogen premixed flame in O2-enriched air condition. Fuel 2020;268:117383. http://dx.doi.org/10.1016/j.fuel.2020.117383.

[10] Lhuillier C, Brequigny P, Contino F, Mounaïm-Rousselle C. Experimental investigation on ammonia combustion behavior in a spark-ignition engine by means of laminar and turbulent expanding flames. Proc Combust Inst 2021;38(4):5859–68. http://dx.doi.org/10.1016/j.proci.2020.08.058.

[11] Zitouni S, Brequigny P, Mounam-Rousselle C. Turbulent flame speed and morphology of pure ammonia flames and blends with methane or hydrogen. Proc Combust Inst 2022. http://dx.doi.org/10.1016/j.proci.2022.07.179.

[12] Wang S, Elbaz AM, Wang Z, Roberts WL. The effect of oxygen content on the turbulent flame speed of ammonia/oxygen/nitrogen expanding flames under elevated pressures. Combust Flame 2021;232:111521. http://dx.doi.org/10.1016/j.combustflame.2021.111521.

[13] Ichimura R, Hadi K, Hashimoto N, Hayakawa A, Kobayashi H, Fujita O. Extinction limits of an ammonia/air flame propagating in a turbulent field. Fuel 2019;246:178–86. http://dx.doi.org/10.1016/j.fuel.2019.02.110.

[14] Dai H, Wang J, Cai X, Su S, Zhao H, Huang Z. Lewis number effects on laminar and turbulent expanding flames of NH3/H2/air mixtures at elevated pressures. Proc Combust Inst 2023;39(2):1689–97. http://dx.doi.org/10.1016/j.proci.2022.07.200.

[15] Zhang R, Chen L, Wei H, Li J, Chen R, Pan J. Understanding the difference in combustion and flame propagation characteristics between ammonia and methane using an optical SI engine. Fuel 2022;324:124794. http://dx.doi.org/10.1016/j.fuel.2022.124794.

[16] Li J, Zhang R, Pan J, Wei H, Shu G, Chen L. Ammonia and hydrogen blending effects on combustion stabilities in optical SI engines. Energy Convers Manage 2023;280:116827. http://dx.doi.org/10.1016/j.enconman.2023.116827.

[17] Uddeen K, Tang Q, Shi H, Turner J. Performance and emission analysis of ammonia-ethanol and ammonia-methane dual-fuel combustion in a spark-ignition engine: An optical study. Fuel 2024;358:130296. http://dx.doi.org/10.1016/j.fuel.2023.130296.

[18] Lhuillier C, Brequigny P, Contino F, Mounaïm-Rousselle C. Experimental study on ammonia/hydrogen/air combustion in spark ignition engine conditions. Fuel 2020;269:117448. http://dx.doi.org/10.1016/j.fuel.2020.117448.

[19] Mercier A, Mounaïm-Rousselle C, Brequigny P, Bouriot J, Dumand C. Improvement of SI engine combustion with ammonia as fuel: Effect of ammonia dissociation prior to combustion. Fuel Commun 2022;11:100058. http://dx.doi.org/10.1016/j.jfueco.2022.100058.

[20] Wüthrich S, Cartier P, Süess P, Schneider B, Obrecht P, Herrmann K. Optical investigation and thermodynamic analysis of premixed ammonia dual-fuel combustion initiated by dodecane pilot fuel. Fuel Commun 2022;12:100074. http://dx.doi.org/10.1016/j.jfueco.2022.100074.

[21] Herrmann K, Wüthrich S, Cartier P, Süess P, de Moura R, Weisser G. Initial investigations into ammonia combustion at conditions relevant for marine engines. In: 30th CIMAC World Congress. 2023.

[22] Li Y, Zhao H, Peng Z, Ladommatos N. Particle image velocimetry measurement of in-cylinder flow in internal combustion engines-experiment and flow structure analysis. Proc Inst Mech Eng D 2002;216(1):65–81. http://dx.doi.org/10.1243/0954407021528913.

[23] Baum E, Peterson B, Böhm B, Dreizler A. On the validation of LES applied to internal combustion engine flows: Part 1: Comprehensive experimental database. Flow Turbul Combust (formerly Appl Scient Res) 2014;92(1–2):269–97. http://dx.doi.org/10.1007/s10494-013-9468-6.

[24] Aleiferis PG, Behringer MK, Malcolm JS. Integral length scales and time scales of turbulence in an optical spark-ignition engine. Flow Turbul Combust (formerly Appl Scient Res) 2017;98(2):523–77. http://dx.doi.org/10.1007/s10494-016-9775-9.

[25] Bradley D, Haq MZ, Hicks RA, Kitagawa T, Lawes M, Sheppard C, et al. Turbulent burning velocity, burned gas distribution, and associated flame surface definition. Combust Flame 2003;133(4):415–30. http://dx.doi.org/10.1016/S0010-2180(03)00039-7.

[26] Goodwin DG, Speth RL, Moffat HK, Weber BW. Cantera: An object-oriented software toolkit for chemical kinetics, thermodynamics, and transport processes. Zenodo; 2021, http://dx.doi.org/10.5281/ZENODO.4527812.

[27] Stagni A, Arunthanayothin S, Dehue M, Herbinet O, Battin-Leclerc F, Bréquigny P, et al. Low- and intermediate-temperature ammonia/hydrogen oxidation in a flow reactor: Experiments and a wide-range kinetic modeling. Chem Eng J 2023;471:144577. http://dx.doi.org/10.1016/j.cej.2023.144577.

[28] Szanthoffer A, Papp M, Kawka L, Zsély IG, Turányi T. Quantitative evaluation of the performances of detailed combustion mechanisms on neat NH3 and NH3/H2 combustion. In: 2nd Symposium on Ammonia Energy. 2023.

[29] Zhang X, Yalamanchi KK, Mani Sarathy S. Combustion chemistry of ammonia/C1 fuels: A comprehensive kinetic modeling study. Fuel 2023;341:127676. http://dx.doi.org/10.1016/j.fuel.2023.127676.

[30] Bertolino A, Fürst M, Stagni A, Frassoldati A, Pelucchi M, Cavallotti C, et al. An evolutionary, data-driven approach for mechanism optimization: theory and application to ammonia combustion. Combust Flame 2021;229:111366. http://dx.doi.org/10.1016/j.combustflame.2021.02.012.

[31] Otomo J, Koshi M, Mitsumori T, Iwasaki H, Yamada K. Chemical kinetic modeling of ammonia oxidation with improved reaction mechanism for ammonia/air and ammonia/hydrogen/air combustion. Int J Hydrog Energy 2018;43(5):3004–14. http://dx.doi.org/10.1016/j.ijhydene.2017.12.066.

[32] Han W, Dai P, Gou X, Chen Z. A review of laminar flame speeds of hydrogen and syngas measured from propagating spherical flames. Appl Energy Combust Sci 2020;1–4:100008. http://dx.doi.org/10.1016/j.jaecs.2020.100008.

[33] Bagheri G, Ranzi E, Pelucchi M, Parente A, Frassoldati A, Faravelli T. Comprehensive kinetic study of combustion technologies for low environmental impact: MILD and OXY-fuel combustion of methane. Combust Flame 2020;212:142–55. http://dx.doi.org/10.1016/j.combustflame.2019.10.014.

[34] Peters N. Turbulent combustion. Cambridge University Press; 2010, http://dx.doi.org/10.1017/CBO9780511612701.

[35] Bechtold JK, Matalon M. The dependence of the Markstein length on stoichiometry. Combust Flame 2001;127(1–2):1906–13. http://dx.doi.org/10.1016/S0010-2180(01)00297-8.

[36] Dinkelacker F, Manickam B, Muppala S. Modelling and simulation of lean premixed turbulent methane/hydrogen/air flames with an effective Lewis number approach. Combust Flame 2011;158(9):1742–9. http://dx.doi.org/10.1016/j.combustflame.2010.12.003.

[37] Beeckmann J, Hesse R, Kruse S, Berens A, Peters N, Pitsch H, et al. Propagation speed and stability of spherically expanding hydrogen/air flames: Experimental study and asymptotics. Proc Combust Inst 2017;36(1):1531–8. http://dx.doi.org/10.1016/j.proci.2016.06.194.

[38] Bouvet N, Halter F, Chauveau C, Yoon Y. On the effective Lewis number formulations for lean hydrogen/hydrocarbon/air mixtures. Int J Hydrog Energy 2013;38(14):5949–60. http://dx.doi.org/10.1016/j.ijhydene.2013.02.098.

[39] Kanoshima R, Hayakawa A, Kudo T, Okafor EC, Colson S, Ichikawa A, et al. Effects of initial mixture temperature and pressure on laminar burning velocity and Markstein length of ammonia/air premixed laminar flames. Fuel 2022;310:122149. http://dx.doi.org/10.1016/j.fuel.2021.122149.

[40] Mounaïm-Rousselle C, Bréquigny P, Dumand C, Houillé S. Operating limits for ammonia fuel spark-ignition engine. Energies 2021;14(14):4141. http://dx.doi.org/10.3390/en14144141.

[41] Mørch CS, Bjerre A, Gøttrup MP, Sorenson SC, Schramm J. Ammonia/hydrogen mixtures in an SI-engine: Engine performance and analysis of a proposed fuel system. Fuel 2011;90(2):854–64. http://dx.doi.org/10.1016/j.fuel.2010.09.042.

[42] Mei B, Zhang J, Shi X, Xi Z, Li Y. Enhancement of ammonia combustion with partial fuel cracking strategy: Laminar flame propagation and kinetic modeling investigation of NH3/H2/N2/air mixtures up to 10 atm. Combust Flame 2021;231:111472. http://dx.doi.org/10.1016/j.combustflame.2021.111472.

[43] Han X, Wang Z, He Y, Zhu Y, Lin R, Konnov AA. Uniqueness and similarity in flame propagation of pre-dissociated NH3 + air and NH3 + H2 + air mixtures: An experimental and modelling study. Fuel 2022;327:125159. http://dx.doi.org/10.1016/j.fuel.2022.125159.